Nanoscale Advances

ROYAL SOCIETY OF CHEMISTRY

PAPER

View Article Online
View Journal | View Issue

Cite this: *Nanoscale Adv.*, 2023, **5**, 5476

Atomic-scale study of TiO_2-GR nanohybrid formation by ALD: the effect of the gas phase precursor†

Jonathan E. Rodríguez-Hueso,[ab] H. A. Borbón-Nuñez, *[bc] R. Ponce-Pérez,[b] D. M. Hoat,[de] N. Takeuchi,[b] H. Tiznado[b] and Jonathan Guerrero-Sánchez*[b]

Received 4th September 2023
Accepted 7th September 2023

DOI: 10.1039/d3na00729d

rsc.li/nanoscale-advances

In the present work, we report on a theoretical-computational study of the growth mechanism of the TiO_2-Graphene nanohybrid by atomic layer deposition. Hydroxyl groups (OH) are anchoring sites for interacting with the main ALD titanium precursors (Tetrakis (dimethylamino) Titanium, Titanium Tetrachloride, and Titanium Isopropoxide). Results demonstrate that the chemical nature of the precursor directly affects the reaction mechanism in each ALD growth step. Tetrakis(dimethylamino)titanium is the precursor that presents a higher affinity (lower energy barriers for the reaction) to hydroxylated graphene in the growth process. A complete reaction mechanism for each precursor was proposed. The differences between precursors were discussed through the non-covalent interactions index. Finally, the water molecules help reduce the energy barriers and consequently favor the formation of the TiO_2-graphene nanohybrid.

1. Introduction

The key to the progress of physical and chemical sciences is understanding and manipulating the properties at the atomic scale. Studying the chemical reactions that allow us to manipulate matter has become fundamental to scientific development.[1] Nanoscience is a set of methods and techniques to treat matter and obtain novel functionalities and improved characteristics.[2,3]

Nanoscale functional hybrid materials are promising in chemistry. These are synthetic materials with organic and inorganic components linked by either non-covalent or covalent bonds.[4] The limitless combinations of the different properties of inorganic, organic, or bioactive components in a single nanoscale material have attracted considerable attention.[5] This approach allows one to create advanced materials with well-controlled structures and multiple functionalities. The unique properties of advanced hybrid nanomaterials can be advantageous in many fields, such as optical and electronic materials, biomaterials, catalysis, sensing, coating, and energy storage.[4,6]

Titanium dioxide (TiO_2) is a metal oxide used to develop photoactive materials for solar energy conversion. It shows efficient photo activity, higher photo-corrosion stability, and low cost.[7–9] Due to its high specific energy density and abundant availability, TiO_2 is also a promising material for supercapacitors, sensors, and other electronic, chemical sensing, and energy storage devices.[10–12] However, the low conductivity of TiO_2 is the main obstacle to developing advanced optoelectronic materials. TiO_2 nanoparticle-based organic hybrids can enhance the conductivity for developing future optoelectronic materials.[13]

Graphene possesses zero band gap and is not chemically reactive, restricting its use in semiconductor devices and sensors.[14] It is possible to modify its electronic and chemical properties through functionalization; surface coatings with different functional groups and couplings in heterostructures become very relevant in building hybrid materials with a high range of applications.[14,15]

The hybrid titanium dioxide-graphene (TiO_2-GR) is a new nanomaterial with improved properties, increasing its potential applications.[16] This nanocomposite is very attractive for manufacturing inorganic compounds with GR matrices thanks to its unique electronic properties, high transparency, flexible structure, and large theoretical specific surface area.[17–19] Among the improvements, the high surface area makes GR beneficial to improving the interfacial contact in the compound; likewise, the doped inorganic TiO_2 nanostructure can prevent the re-aggregation of exfoliated GR sheets, maintaining the

[a]*Centro de Investigación Científica y de Educación Superior de Ensenada,Carretera, Tijuana-Ensenada 3918, Apdo. Postal 22860, Ensenada, B.C., Mexico*

[b]*Centro de Nanociencias y Nanotecnología, Universidad Nacional Autónoma de México, Km.107, Apdo. Postal 14. Carretera Tijuana-Ensenada, Ensenada, Baja California, Mexico. E-mail: hborbon@ens.cnyn.unam.mx; guerrero@ens.cnyn.unam.mx*

[c]*CONAHCyT- Centro de Nanociencias y Nanotecnología, Universidad Nacional Autónoma de México, Km.107, Apdo. Postal 14. Carretera Tijuana-Ensenada, Ensenada, Baja California, Mexico*

[d]*Institute of Theoretical and Applied Research, Duy Tan University, Ha Noi 100000, Viet Nam*

[e]*Faculty of Natural Sciences, Duy Tan University, Da Nang 550000, Viet Nam*

† Electronic supplementary information (ESI) available. See DOI: https://doi.org/10.1039/d3na00729d

performance of GR.[20–22] Furthermore, since GR has excellent physical and chemical properties, TiO_2-carbon compounds can also show good photocatalytic activity under UV light.[23] Therefore, compared to the pure materials, GR-based nanocomposites exhibit improved activities due to the synergistic effect of the GR and TiO_2 components.[17,24]

Some typical manufacturing methods for TiO_2-GR nanohybrids are the hydrothermal method, the solvent method, the self-assembly method, the electro-spinning method, and atomic layer deposition (ALD).[25] ALD, formerly known as atomic layer epitaxy, is a technique that enables a layer-by-layer growth of metallic, oxide, sulfide, and nitride films onto the surface of materials.[26–28] ALD is crucial in manufacturing various devices and is part of the tools available for synthesizing nanomaterials.[29,30] Most ALD reactions use two chemicals called precursors or reactants. These precursors react with the surface of a material, one at a time, sequentially, and self-limitedly. Through repeated exposure to separate precursors, a thin film is homogeneously deposited. In the case of the TiO_2-GR hybrid, the most used precursors as titanium source are:[31–34] Tetrakis (dimethylamino) titanium (TDMAT) $Ti[(CH_3)_2N]_4$, Titanium tetrachloride (TTC): $TiCl_4$, and Titanium isopropoxide (TIP): $Ti[OCH(CH_3)_2]_4$

Having a chemically reactive surface is very important in ALD growth.[35] However, graphene (like other substrate materials) is not chemically reactive, restricting the ALD nucleation process. Hydroxylation, through different physical and chemical methods, improves nucleation.[14] A hydroxyl-terminated surface reacts more readily with many ALD precursors, resulting in a more complete reaction with the graphene surface, thus improving the nucleation.[28] In these cases, the surface hydroxyl groups play an important role because they take place as the anchoring sites or growth zones to achieve the reaction with the precursor molecules.[35]

The high precision provided by the ALD technique and an atomic-scale film growth control makes ALD the ideal method to study the nucleation and growth of nanocomposite materials at the atomic scale.[34] One of these methods is to use Quantum mechanical calculations based on the density functional theory (DFT)[36,37] to develop a model of the chemistry involved in the reactions that occur in the ALD processes during the growth stages of TiO_2-GR hybrid nanofilms.[38–40]

In this paper, we demonstrate that the chemical nature of the precursor directly affects the TiO_2 ALD growth on hydroxylated graphene through a theoretical-computational study. The minimum energy pathways and the non-covalent interactions index (NCI) helps describe and compare the TiO_2 growth using three main ALD titanium precursors (TDMAT, TIP, TTC) and their interactions with the hydroxylated graphene nanostructure.

2. Computational method

We have used spin-unrestricted quantum mechanical calculations to describe the TDMAT, TIP, and TTC adsorption and the initial stages of the TiO_2 formation on hydroxyl functionalized graphene. Calculations based on Density Functional Theory[41] have been used, as implemented in the PWscf code of the Quantum ESPRESSO package.[42,43] The electronic states and charge density have been expanded in plane waves with kinetic energy and charge density cutoffs of 40 Ry and 320 Ry, respectively. The exchange–correlation interactions have been modeled by using the generalized gradient approximation, as stated by Perdew–Burke–Ernzerhof (PBE).[41,44] Ultrasoft pseudopotentials consider the ion–electron interactions.[45] The valence configurations for the atomic species are C-$2s^2$ $2p^2$, Ti-$4s^2$ $3d^2$, and O–$2_s{}^2 2p^4$. Grimme-D3 long-range dispersion corrected interactions are accounted for to describe the solid–gas interactions.[46] The energy convergence criterion was set to 1×10^{-4} Ry. The graphene unit cell has a lattice parameter $a = 2.46$ Å, with interatomic distance ~1.42 Å.[47] We used 4×4 (when treating TDMAT and TTC) and 5×5 (in the case of TIP) graphene supercells. Different periodicities will result in similar results since the ALD reaction is localized at the active OH sites. The length of the supercell along z direction was optimized to 10 Å. This length is large enough to preclude interaction between neighbor molecules.[48–51] Climbing Image Nudged Elastic Band (CI-NEB) calculations were applied to obtain the different ALD reaction steps' minimum energy pathways (MEP).[52]

3. Results and discussion

First, we calculate the structure of the three titanium precursors and compare them with the already reported structures. Also, hydroxylated graphene was constructed considering a vacancy defect in which the remaining C dangling bonds are saturated by hydrogen atoms to just consider the hydroxyl effect on the ALD reactions[53–55] (see Fig. S1(a–d), ESI†).

The next step is to evaluate the precursor-hydroxylated graphene interaction in the different ALD growth steps. ALD comprises two half-cycles, the first in which the organometallic precursor arrives at the functionalized substrate and the second in which the oxidizing agent reacts with the surface-attached metallic precursor molecule.

3.1 First half ALD cycle

In the first ALD half cycle, we evaluated the interaction between the precursor molecules with the hydroxylated graphene (GR(OH)) surface. Here, we describe the ligand exchange reaction for each precursor; these are:

TDMAT

$$\text{Ti-}[N(CH_3)_2]_4 + |GR|\text{-OH} \rightarrow |GR|\text{-O-Ti-}[N(CH_3)_2]_3 + NH(CH_3)_2 \quad (1a)$$

TTC

$$TiCl_4 + |GR|\text{-OH} \rightarrow Ti(Cl_3)\text{-O-}|GR| + HCl \quad (1b)$$

TIP

$$\text{Ti-}[O\text{–}CH(CH_3)_2]_4 + |GR|\text{-OH} \rightarrow |GR|\text{-O-Ti-}[O\text{-}CH(CH3)_2]_3 + (OH)\text{-}CH(CH_3)_2 \quad (1c)$$

In GR(OH)-TDMAT (see Fig. 1a), we can observe the ligand exchange between the hydroxyl group of the GR surface and one amine group of the TDMAT molecule. In the GR(OH)-TTC reaction (see Fig. 1b), the ligand exchange happens with one chlorine atom of the TCC molecule. Finally, for the GR(OH)-TIP reaction (Fig. 1c), the ligand exchange occurs between the one isopropyl group from the TIP molecule and the OH on the surface. The reaction products obtained for the TDMAT, TTC, and TIP are dimethylamine, hydrochloric acid, and isopropyl alcohol. Similar reaction products have been observed previously in ALD reactions[55–58]. The main difference was the atomic species interaction with the hydroxylated graphene surface ([N–H] for TDMAT, [Cl–H] for TTC, and [O–H] for TIP), and the position of the precursor molecules to generate the interactions, being governed by steric hindrance and attraction between the species according to the chemical nature of each precursor. In each case, a Ti–O bond appears.

3.2 First half ALD cycle: reactions pathways

To evaluate the viability of the first half ALD cycle, we proceed to evaluate the minimum energy pathway (MEP) of each ligand exchange reaction. The first half cycle has three steps. The initial step (IS) is when the organometallic precursor interacts with the GR(OH). The intermediate step is the energy barrier to achieve the ligand-exchange reaction—the final step (FS) is the reaction product generation. Fig. 2 depicts the minimum energy pathway to achieve the FS for each precursor.

For TDMAT, notice that the ligand-exchange occurs almost with no energy barrier ($TS_{TDMAT} = 0.01$ eV). Also, to achieve FS, the system gains energy (−0.64 eV), which is the most probable scenario if all precursors are competing. For TTC and TIP, the energy barriers are higher ($TS_{TTC} = 0.77$ eV and $TS_{TIP} = 0.65$ eV), respectively. Compared with some of the few works related to the MEPs of these reactions, the behavior of the energetic barriers is the same. The energy barrier to go further with the reaction occurs when the ligand exchange between the precursor and the surface hydroxyl group is generated. In our case, only one hydroxyl group was used to elucidate and compare the behavior between precursors.[56,58–60] The ligand-exchange reactions calculated could happen in the following order, TDMAT < TIP < TTC. Our calculations follow the well-known temperature tendency for the titanium precursors, where the reaction temperature follows the order TDMAT < TIP < TTC,[49,55] see Fig. S2.† Here we can relate the obtained energy barriers with the temperature reported for the deposition of each precursor, since it is the energy required to turn on the reactions in the TiO_2 ALD growth. So, our calculations show that TDAMT is more efficient in the first ALD half-reaction.

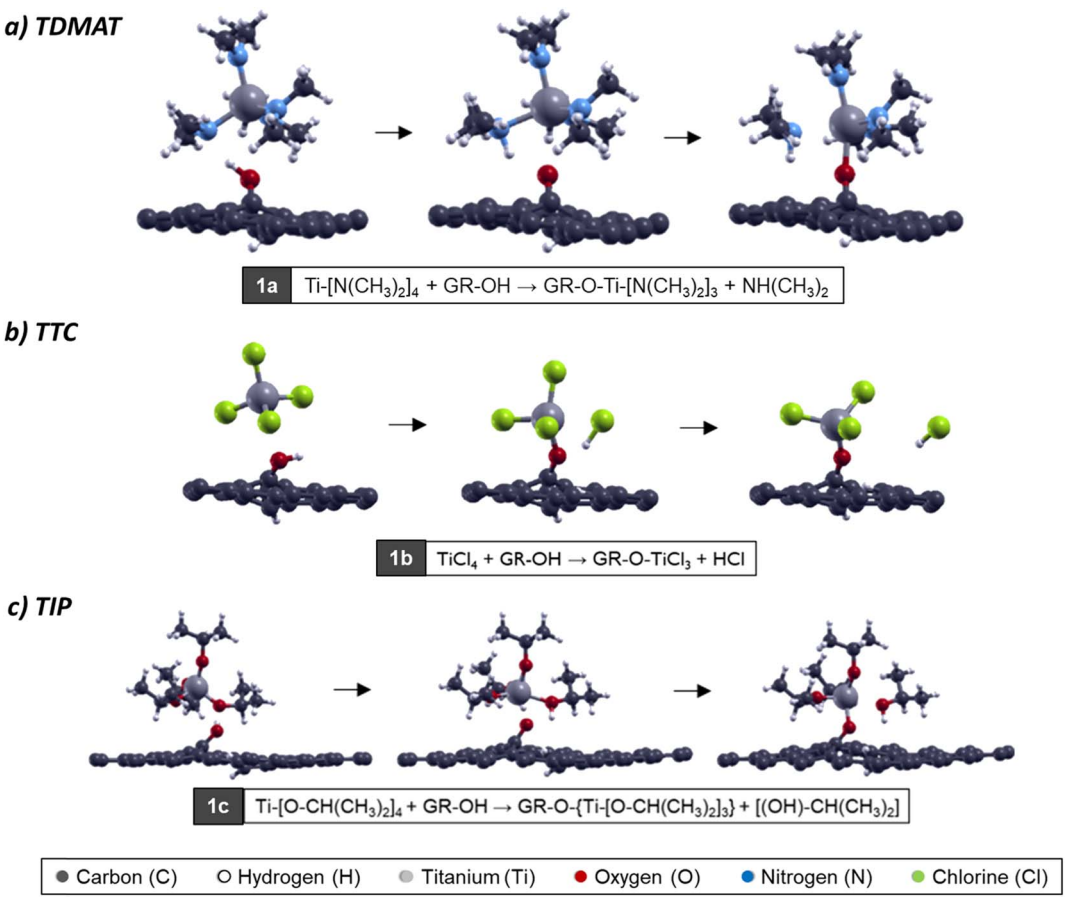

Fig. 1 Atomic model of TDMAT (a), TTC (b), and TIP (c) precursors interacting with the OH functionalized graphene nanostructure on the 1st ALD step.

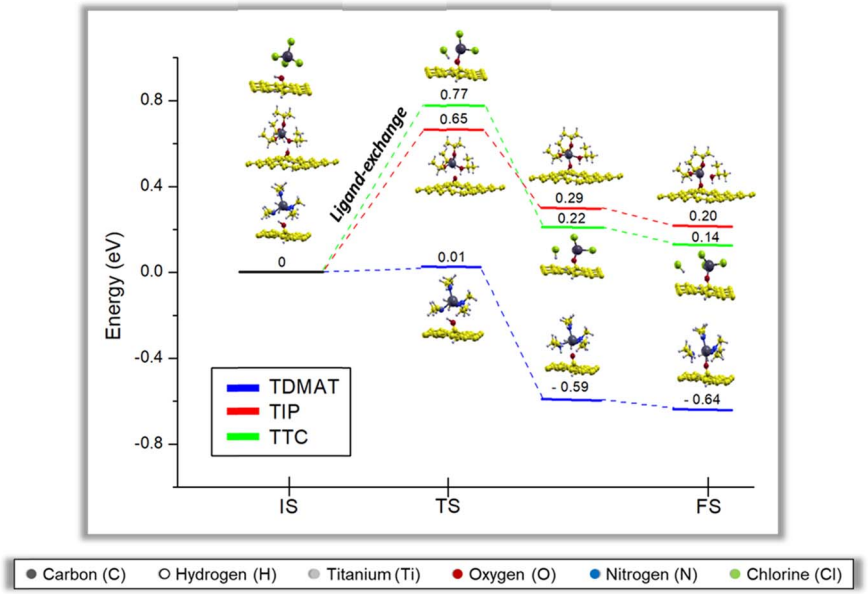

Fig. 2 Minimum energy pathways for the 1st ALD half cycle.

3.3 Second half ALD cycle

After the first ALD cycle, the system goes under a purge to eliminate all the unreacted precursors and the reaction products in each case (dimethylamine from TDMAT, hydrochloric acid from TTC, and isopropyl alcohol from TIP). After that, the second half ALD cycle begins. Here the substrate is exposed to an oxidizing agent, where H_2O molecules are the most employed experimentally.[56,58,59] The reactions that take place are:

TDMAT

$$|GR|\text{-O-Ti-}[N(CH_3)_2]_3 + H_2O \rightarrow |GR|\text{-O-}\{(OH)\text{-Ti-}[N(CH_3)_2]_2\} + NH(CH_3)_2 \quad (2a)$$

TTC

$$|GR|\text{-O-}TiCl_3 + H_2O \rightarrow |GR|\text{-O-}\{(Cl_2)\text{-Ti-}(OH)\} + HCl \quad (2b)$$

TIP

$$|GR|\text{-O- Ti-}[O\text{-}CH(CH3)_2]_3 + H_2O \rightarrow |GR|\text{-O-}\{(OH)\text{-Ti-}[O\text{-}CH(CH_3)_2]_2\} + (OH)\text{–}CH(CH_3)_2 \quad (2c)$$

From an atomistic point of view, we evaluated the interaction between the surface obtained in the first ALD step with a water molecule. In this reaction, we appreciate the oxidation in the surface, where the water approached and generated the ligand-exchange. This process happens for each precursor, and the ligand-exchange is like the first step. We have the same reaction products (dimethylamine from TDMAT, hydrochloric acid from TTC, and isopropyl alcohol from TIP).[55–58]

For the oxidation process, when TDMAT is chemisorbed on the surface (GRO-TDMAT), the ligand exchange occurs when the H_2O molecule approaches the surface. It generates interaction with an amine group through one nitrogen atom, breaking the water molecule (see Fig. 3a). For the case of GRO-TTC surface oxidation, the interaction happens between the oxygen in the H_2O and the titanium atom directly (Fig. 3b); the water molecule tilts, and the H from H_2O interacts with the chlorine atom, breaking the bonds and generating the ligand-exchange. Finally, for GRO-TIP oxidation (Fig. 3c), the ligand-exchange occurs as in the TTC case; the water molecule approaches the titanium atom and then generates the ligand-exchange with an isopropyl group on the TIP molecule. After this step, the second bond between Ti and OH group appears.

3.3.1 Second half ALD cycle: reaction pathways. As in the first ALD cycle, the same tendency is observed; the energy barrier for the ligand exchange in TDMAT (eqn (2a)) is 0.40 eV, while the required energy for the ligand exchange in TTC (eqn (2b)) and TIP (eqn (2c)) is 0.96 eV and 0.80 eV, respectively (see Fig. 4). The minimum energy pathways of the ligand-exchange processes for the H_2O molecule interaction with the different titanium precursors are depicted in Fig. 4. MEP shows that when the water molecule interacts with TDMAT, the reaction proceeds forward in an exothermic process (it gains −0.27 eV). The reactions in TTC and TIP are endothermic since the initial step energy is lower than the final step by 0.46 eV and 0.33 eV, respectively. Similar trends have been reported in the literature for the MEPs, in which the energy barriers are larger than in the first half ALD cycle.[56,58–60] Here the observed energetic trend TDMAT < TTC < TIP remains, so the most efficient precursor to complete the ALD reaction is TDMAT.

3.3.2 Second half ALD cycle: the effect of water molecules. To analyze the second middle ALD cycle, we must focus on the water molecules effect since it has been demonstrated that water molecules interact to efficiently reduce the required energy for the ligand-exchange (in this case, partial water splitting: $H_2O \rightarrow O + OH$). This effect has already been proven

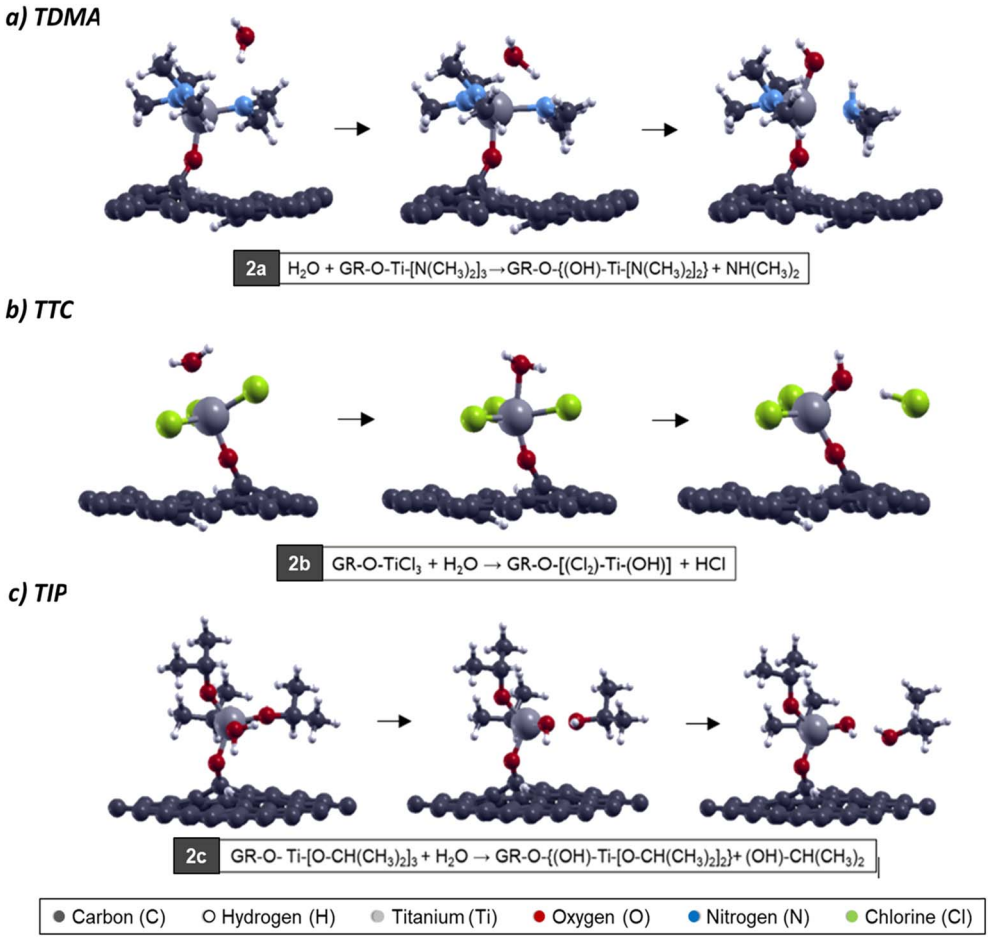

Fig. 3 Atomic model of H_2O molecule interacting with (a) GRO-TDMAT, (b) GRO-TTC, and (c) GRO-TIP surfaces for the second ALD half cycle.

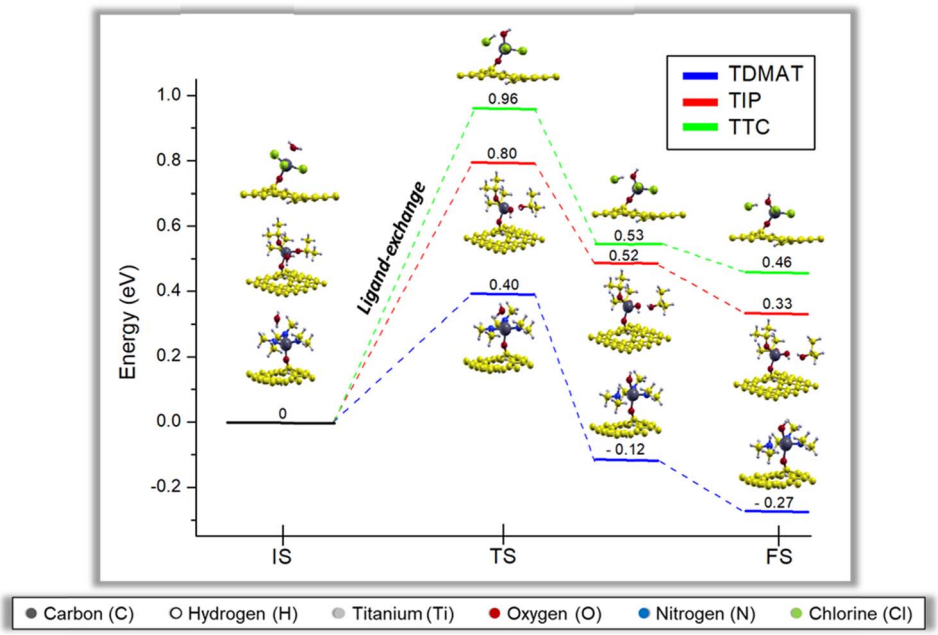

Fig. 4 Minimum energy pathways for the 2nd ALD half cycle with one water molecule.

for the ZnO ALD growth[30] and to generate water splitting in TiO_2 due to the formation of water networks mediated by weak interactions[64]. In this case, we evaluated the effect of water molecules by explicitly adding two water molecules in the second ALD cycle. To do it, we have determined the minimum energy pathways. This oxidation reaction proceeds on the surface in two transition states. The ligand-exchange proceeds in two steps for each water molecule, as in the case of the interaction with one water molecule. The reactions that take place are:

TDMAT

$$|GR|\text{-O-Ti-}[N(CH_3)_2]_3 + 2H_2O \rightarrow |GR|\text{-O-}\{[2(OH)]\text{-Ti-}[N(CH3)_2]\} + 2[NH(CH_3)_2] \quad (3a)$$

TTC

$$|GR|\text{-O-}TiCl_3 + 2H_2O \rightarrow |GR|\text{-O-}\{Cl\text{-Ti-}[2(OH)]\} + 2HCl \quad (3b)$$

TIP

$$|GR|\text{-O-Ti-}[O\text{-}CH(CH_3)_2]_3 + 2H_2O \rightarrow |GR|\text{-O-}\{[2(OH)]\text{-Ti-}[O\text{-}CH(CH_3)_2]\} + 2[(OH)\text{–}CH(CH_3)_2] \quad (3c)$$

For the oxidation on the GRO-TDMAT surface, the ligand exchange occurs when the two H_2O molecules approach the surface, generating a weak interaction with one nitrogen atom in an amine group, breaking the water molecule (see Fig. 5a). For the case of the oxidation of (GRO-TTC)-H_2O surface (Fig. 5b), the interaction happens between the oxygen in the water and the titanium directly. In the second step, the water molecule tilts, and the hydrogen in the water molecule interacts with the chlorine atom, further breaking the bonds and generating the ligand exchange. Finally, for the oxidation of GRO-TIP (Fig. 5c), the ligand exchange occurs similarly as in TDMAT; the water molecules approach the surface generating the exchange with the isopropyl groups of the TIP molecule.

3.4 Reactions pathways

Fig. 6 reports the minimum energy pathway in the second middle ALD cycle, including two water molecules. The behavior is like the one water molecule case, but two energy barriers exist related to breaking both water molecules. The water molecules effect has also been discussed in the previous reports; they show that each water molecule generates a ligand exchange (energy barrier) with the available groups of the precursors, a result consistent with our findings for the case of one and two water molecules in the second half ALD cycle[58–60]. Notice that the existence of two water molecules diminishes the energy barrier (TS1) in the first step due to a synergistic effect between water molecules, which may be forming hydrogen bonds between

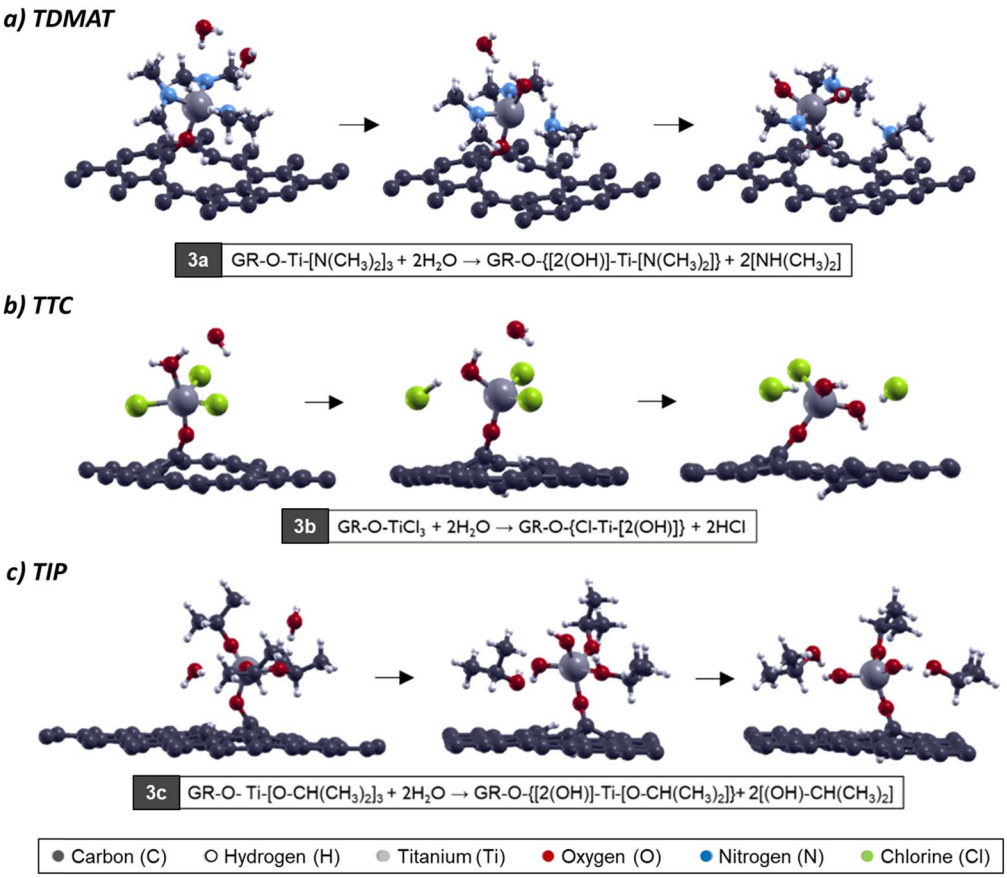

Fig. 5 Atomic model of $2H_2O$ molecule interacting with (a) GRO-TDMAT, (b) GRO-TTC, and (c) GRO-TIP surface for the second ALD half cycle.

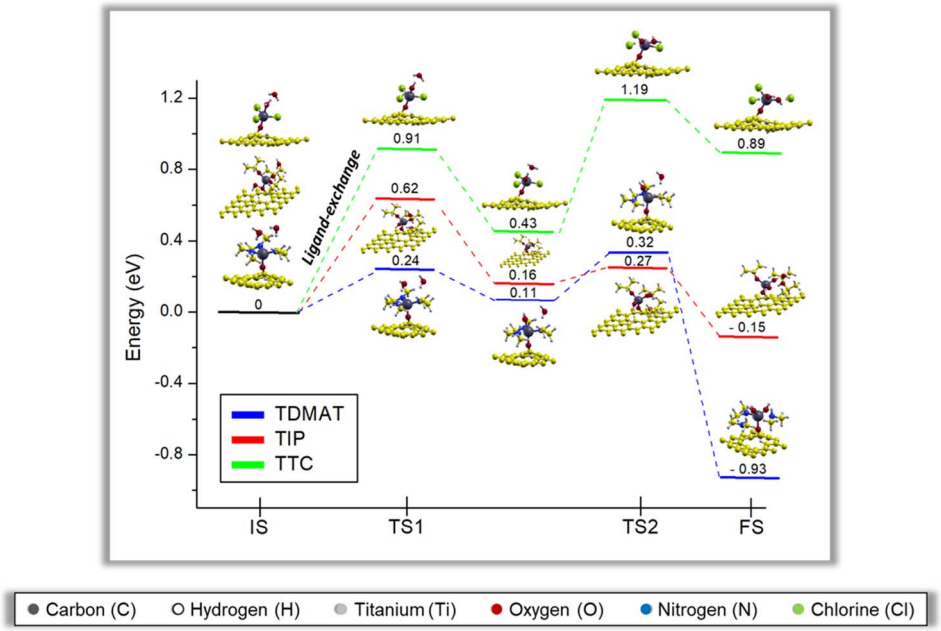

Fig. 6 Minimum energy pathways for the 2nd ALD half cycle with two water molecules.

them to facilitate the first ligand-exchange reaction. For the second ligand-exchange, the energy barrier is lower for TDMAT and TIP, presumably because of reduced steric hindrance. Although the second ligand-exchange is more favorable for TIP than TDMAT, the limiting step of the reaction is the first ligand-exchange, making the process more favorable in TDMAT, see Fig. 6. In contrast, for TTC, the energy barrier increases even more than in the case with one water molecule; this happens because even though water molecules interact, the ligand-exchanges in TTC happen separately, so the water molecules saturation effect is just effective in the first ligand-exchange but not in the second. The non-covalent interactions Section 3.5 will discuss these findings in more detail.

The second middle ALD reaction in the presence of two water molecules for TDMAT and TIP is exothermic, while for TTC is an endothermic reaction. In this case, the energetic trend is TDMAT < TIP < TTC, confirming that the chemical nature of the precursor plays a key role in the initial stages of the TiO_2-GR nanohybrid formation by ALD.

E. Dufond *et al.*[55] observed through an exhaustive physico-chemical characterization that the precursor nature (TIP and TDMAT) critically affects the TiO_2 chemical composition. In agreement with our findings, they evidenced that TDMAT is better in the standard ALD mechanism and attributed such an effect to interactions with the surface OH groups and deposition temperatures. Our theoretical results are consistent with the experiments by E. Dufond *et al.*[55] We also add up the TTC effect, and still, TDMAT remains better suited for the ALD reaction.

3.5 Non-covalent interactions

To better understand the interactions in the ALD cycle, we investigated the non-covalent interactions index (NCI).[61] NCI is useful to differentiate the interactions present in the systems. The reduced density gradient, $s(\rho)$, is defined as follows:[62]

$$s(\rho) = \frac{1}{2(3\pi^2)^{1/3}} \frac{|\nabla\rho(r)|}{\rho(r)^{4/3}}$$

Also, the second eigenvalue (λ_2) of the density Laplacian, $\nabla^2\rho(r)$, takes different values. $\lambda_2 > 0$ stands for not bonded interactions, while negative values ($\lambda_2 < 0$) are for bonded interactions; besides, values close to zero ($\lambda_2 \approx 0$) suggest vdW interactions. Therefore, if we plot $s(\rho)$ as a function of the $\mathrm{sig}(\lambda_2)\rho$, we can observe the non-covalent interactions in the region of low reduced density gradient and low electron density. Also, the strength of the interaction increases as the electron density increases.

Our results show that the viability of using TDMAT as a precursor comes from the first half ALD cycle since the reaction goes forward without energy barriers. Fig. 7a shows the s *vs.* $\mathrm{Sig}(\lambda_2)\rho$ plot for the three different precursors in the IS according to Fig. 2 and their corresponding isosurfaces ($s = 0.5$ a.u.). In the case of TDMAT (black dots), the graph shows the presence of a hydrogen bond (H-bond) between the OH from GR(OH) and one nitrogen from TDMAT characterized by the sharp peak at ±0.07, their corresponding isosurface (lower panel of Fig. 7) corroborates the presence of the H-bond (red isosurface) and the presence of weak interactions (green isosurface) between the amine groups and GR. About TIP molecule, the graph suggests the presence of an H-bond (red dots) between some oxygen from TIP and the GR(OH); however, this H-bond is weaker in comparison to the one observed in TDMAT since the sharp peak that represents is located at 0.06, their corresponding isosurfaces corroborates the presence of the H-bond and the presence of vdW interactions between the GR

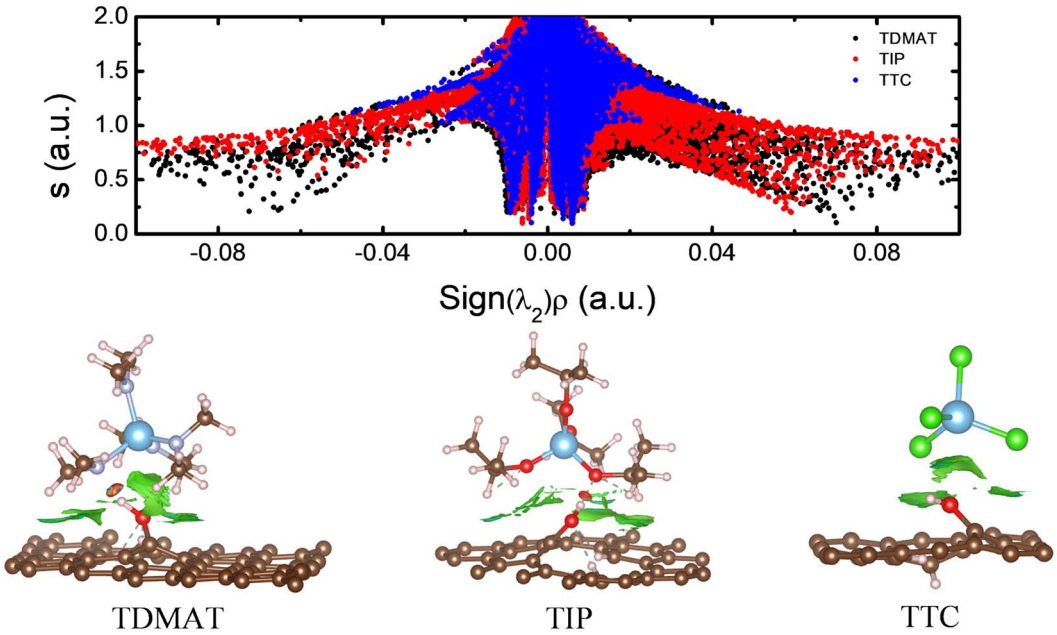

Fig. 7 *s vs.* Sign(λ_2)ρ plot for TDMAT, TIP, and TTC precursors and their corresponding isosurface with $s = 0.5$ a. u.

and the isopropyl groups from the precursor. In the case of TTC (blue dot surface), the s *vs.* Sig(λ_2)ρ plot describes a weak interaction between molecule and GR(OH) observed at low s and low electron density. Also, the isosurface only shows vdW interactions between the molecule and GR(OH). Our results show that a strong interaction between molecule and surface reduces the energy barriers in the minimum energy pathway favoring the use of TDMAT as a precursor of TiO_2.

We also investigated the water effect in the second half ALD cycle for the TDMAT precursor. The upper panel of Fig. 8 shows the s *vs.* Sign(λ_2)ρ graph corresponding to the IS considering one (magenta dots) and two water molecules (orange dots). For an easier comparison, we only plot the interaction between one H_2O and TDMAT in the case of two water molecules. In both cases, the interaction between molecules is similar. The peak at -0.03 corresponds with the attractive interaction between some H from H_2O and one nitrogen from the dimethylamine groups. Also, the peaks close to zero represent the weak interaction between water and neighboring dimethylamine groups. Therefore, more water molecules around TDMAT do not modify their interactions in the IS.

Similarly, the lower panel from Fig. 8 depicts the s *vs.* Sign(λ_2)ρ plot for the TS (TS1) stage for the second half ALD cycle considering one (two) water molecule(s). For the first case,

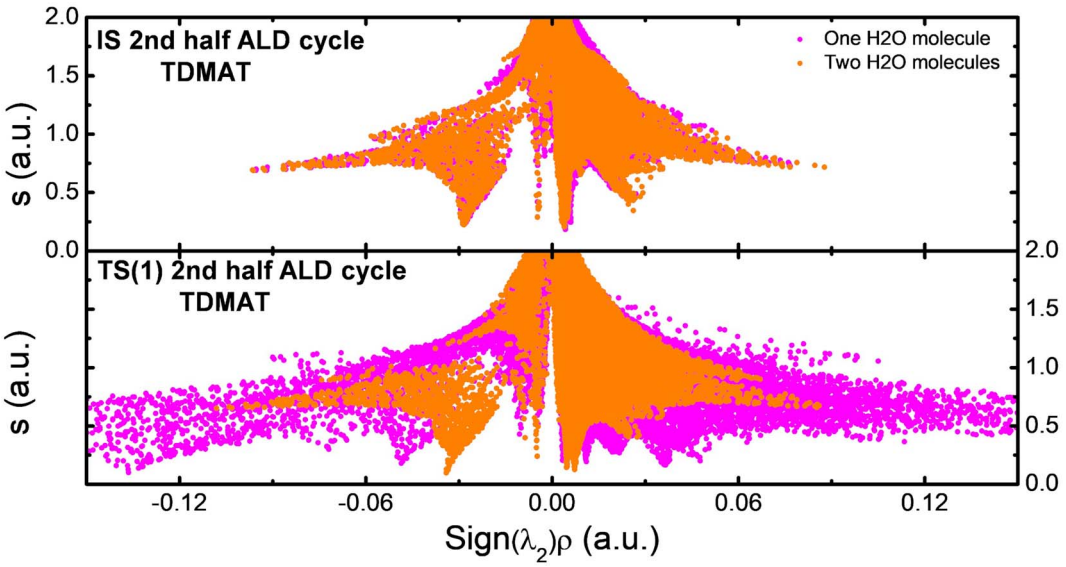

Fig. 8 *s vs.* Sign(λ_2)ρ plot for TDMAT precursor and the corresponding isosurface with $s = 0.5$ a. u.

the sharp peak at −0.13 is associated with the H–N bond formation between one hydrogen from H_2O and the nitrogen from the dimethylamine group. The peak at −0.05 comes from an attractive interaction between the O from H_2O and the titanium from TDMAT. Also, the magenta peaks ranging from −0.01 to 0.05 result from the weak interaction between the H_2O molecule and the neighboring dimethylamine groups. On the other hand, when two water molecules are considered (orange dots), the sharp peak at −0.035 is result of an attractive interaction between the nitrogen from the dimethylamine group and the hydrogen from water, and the three peaks close to zero come from the weak interaction between water and TDMAT. The effect of the second water molecule is clearly seen in the TS1 state since thanks to this molecule the first H_2O avoids interacting with titanium and neighboring dimethylamine groups, reducing the energy barrier in the MEP and then facilitating the first ligand exchange.

4 Conclusions

Through a comprehensive *ab initio* assessment, we have understood the ALD growth of the nanohybrid TiO_2-Grapehene, considering different titanium precursors. Hydroxyl groups are the main anchoring reactive sites for the reactions. Our results demonstrated that the nature of the precursors directly impacts the atomic layer deposition growth. Tetrakis(dimethylamino) titanium is the precursor with the highest affinity, inducing an easy TiO_2-graphene nanohybrid growth at low temperatures. Titanium isopropoxide and titanium tetrachloride precursors activate at higher temperatures and are less efficient for the TiO_2 atomic layer deposition growth. The non-covalent interactions index evidence that hydrogen bonds dominate the reactions. When considering the Tetrakis(dimethylamino)titanium precursor, strong hydrogen bonds appear, thus reducing the energy barriers and driving more efficient growth at low temperatures. Also, the saturation of water molecules improves the reactions in the second half atomic layer deposition cycle for all precursors; however, the tetrakis(dimethylamino)titanium precursor remains the most efficient and with lower energy barriers for the reaction. The evidence generated here helps understand -at an atomic level-the key role that weak interactions play in technologically and industrially relevant processes such as atomic layer deposition. Also, they are a guide to improving the existing experimental procedures.

Conflicts of interest

There are no conflicts to declare.

Acknowledgements

We thank DGAPA-UNAM IA100822, IN105722, IN101523, and Conacyt grants A1-S-9070 and A1-S-26789 of the Call of Proposals for Basic Scientific Research 2017–2018 for partial financial support. Calculations were performed in the DGCTIC-UNAM Supercomputing Center, projects LANCAD-UNAM-DGTIC-368, LANCAD-UNAM-DGTIC-051, LANCAD-UNAM-DGTIC-390, and LANCAD-UNAM-DGTIC-422. We thank Aldo Rodriguez-Guerrero and J. I. Paez-Ornelas for their technical support.

References

1 G. Lusvardi, C. Barani, F. Giubertoni and G. Paganelli, Synthesis and characterization of TiO2 nanoparticles for the reduction of water pollutants, *Materials*, 2017, **10**(10), 1–11.
2 G. Mendoza and J. L. Rodríguez-lópez, La nanociencia y la nanotecnología: una revolución en curso, *Perf. Latinoam.*, 2007, **14**(29), 161–186.
3 N. Munir, *Fundamentals and Applications of Nano Silicon in Plasmonics and Fullerines*, Elsevier, 1st edn, 2018, pp. 139–151.
4 J. L. Dávila, V. H. Guerrero, P. Pontón, N. M. Rosas, V. Sotomayor and C. Valdivieso *Nuevos materiales: aplicaciones estructurales e industriales*, Imprefepp, 1st edn, 2011, p. 35.
5 V. P. Ananikov, Organic–Inorganic Hybrid Nanomaterials, *Nanomaterials*, 2019, **9**(9), 1197.
6 L. H. Liu, R. Métivier, S. Wang and H. Wang, Advanced nanohybrid materials: Surface modification and applications, *J. Nanomater.*, 2012, 1–2.
7 A. J. Haider, R. H. Al-Anbari, G. R. Kadhim and C. T. Salame, Exploring potential environmental applications of TiO2 Nanoparticles, *Energy Procedia*, 2017, **119**, 332–345.
8 A. Listanti, A. Taufiq, A. Hidayat, Sunaryono, N. Hidayat, H. Susanto and S. Soontaranon, Synthesis structural and toxicity characters of nano-sized titanium dioxide/magnetite nanoparticles, *IOP Conf. Ser.: Mater. Sci. Eng.*, 2019, **515**(1), 012057.
9 D. Losic, G. Triani, P. J. Evans, A. Atanacio, J. G. Mitchell and N. H. Voelcker, Controlled pore structure modification of diatoms by atomic layer deposition of TiO2, *J. Mater. Chem.*, 2006, **16**(41), 4029–4034.
10 M. Fernández-García and J. A. Rodriguez, Metal Oxide Nanoparticles, *Encyclopedia of Inorganic Chemistry*, October, 2009.
11 S. S. Al-Taweel and H. R. Saud, New route for synthesis of pure anatase TiO2 nanoparticles *via* ultrasound-assisted sol-gel method, *J. Chem. Pharm. Res.*, 2016, **8**(2), 620–626.
12 N. Martín, M. Viniegra, R. Vargas and J. Garza, Nanostructured oxides of transition metals with applications in catalysis, *Mundo nano, Revista interdisciplinaria en nanociencias y nanotecnología*, 2021, **14**(26), 1–16.
13 L. P. L. Mawlong, K. K. Paul and P. K. Giri, Direct Chemical Vapor Deposition Growth of Monolayer MoS2 on TiO2 Nanorods and Evidence for Doping-Induced Strong Photoluminescence Enhancement, *J. Phys. Chem. C*, 2018, **122**(26), 15017–15025.
14 S. Robin and A. Kottantharayil, Stable hydroxyl functionalization and p-type doping of graphene by a non-destructive photo-chemical method, *Carbon*, 2019, **152**, 267–273.

15 F. Buonocore, C. Andrea, M. Celino, N. Lisi and P. Olivia, Tuning the Electronic Properties of Graphane *via* Hydroxylation: An *Ab Initio* Study, *J. Phys. Chem. C*, 2021, **125**(29), 16316–16323.
16 K. Pathakoti, M. Manubolu and H. M. Hwang, Nanostructures: Current uses and future applications in food science, *J. Food Drug Anal.*, 2017, **25**(2), 245–253.
17 X. Yu, D. Lin, P. Li and Z. Su, Recent advances in the synthesis and energy applications of TiO2-graphene nanohybrids, *Sol. Energy Mater. Sol. Cells*, 2017, **172**(May), 252–269.
18 Z. Anwar, A. Kausar, I. Rafique and B. Muhammad, Advances in Epoxy/Graphene Nanoplatelet Composite with Enhanced Physical Properties: A Review, *Polym.-Plast. Technol. Eng.*, 2016, **55**(6), 643–662.
19 E. Araque Caballero, *Nanomateriales híbridos de óxido de grafeno y polímeros hidrosolubles para el diseño de plataformas biosensoras electroquímicas*, Doctoral thesis, Universidad complutense de Madrid, 2015, pp. 25–32.
20 A. C. Ferrari, F. Bonaccorso, V. Falko, K. S. Novoselov, S. Roche, P. Bøggild, A. Borini and E. Ballerini, Science and technology roadmap for graphene, related two-dimensional crystals, and hybrid systems, *Nanoscale*, 2015, **7**(11), 4598–4810.
21 B. D. Ossonon and D. Bélanger, Synthesis and characterization of sulfophenyl-functionalized reduced graphene oxide sheets, *RSC Adv.*, 2017, **7**(44), 27224–27234.
22 J. G. Suárez Guevara, *Materiales híbridos basados en nanocarbones y polioxometalatos para aplicación como electrodos en supercoductores con mecanismo dual de amacenamiento de energía*, Doctoral thesis, Universidad Autonoma de Barcelona. España, 2014, **http://hdl.handle.net/10803/285650**.
23 L. L. Tan, W. J. Ong and S. P. Chai, Reduced graphene oxide-TiO_2 nanocomposite as a promising visible-light-active photocatalyst for the conversion of carbon dioxide, *Nanoscale Res. Lett.*, 2013, **8**, 465.
24 X. Liu, R. Yan, J. Zhu, J. Zhang and X. Liu, Growing TiO2 nanotubes on graphene nanoplatelets and applying the nanonanocomposite as scaffold of electrochemical tyrosinase biosensor, *Sens. Actuators, B*, 2015, **209**, 328–335.
25 E. Kusiak-Nejman and A. W. Morawski, TiO2/graphene-based nanocomposites for water treatment: A brief overview of charge carrier transfer, antimicrobial and photocatalytic performance, *Appl. Catal., B*, 2019, **253**, 179–186.
26 V. Cremers, R. L. Puurunen and J. Dendooven, Conformality in atomic layer deposition: Current status overview of analysis and modelling, *Applied Physics Reviews*, 2019, **6**(2), 021302.
27 H. Tiznado, D. Domínguez, F. Muñoz-Muñoz, J. Romo-Herrera, R. Machorro, O. E. Contreras and G. Soto, Pulsed-bed atomic layer deposition setup for powder coating, *Powder Technol.*, 2014, **267**, 201–207.
28 A. F. Palmstrom, P. K. Santra and S. F. Bent, Atomic layer deposition in nanostructured photovoltaics: tuning optical, electronic and surface properties, *Nanoscale*, 2015, **7**(29), 12266–12283.
29 R. W. Johnson, A. Hultqvist and S. F. Bent, A brief review of atomic layer deposition: From fundamentals to applications, *Mater. Today*, 2014, **17**(5), 236–246.
30 J. I. Paez-Ornelas, H. N. Fernández-Escamilla, H. A. Borbón-Nuñez, H. Tiznado, N. Takeuchi and J. A. Guerrero-Sánchez, First-principles study of the atomic layer deposition of ZnO on carboxyl functionalized carbon nanotubes: The role of water molecules, *Phys. Chem. Chem. Phys.*, 2021, **23**(5), 3467–3478.
31 A. Zydor and S. D. Elliott, TiCp*(OMe) 3 *versus* Ti(OMe) 4 in atomic layer deposition of TiO 2 with water - *Ab initio* modelling of atomic layer deposition surface reactions, *J. Nanosci. Nanotechnol.*, 2011, **11**(9), 8089–8093.
32 H. A. Borbón-Nuñez, J. Muñiz, A. G. El Hachimi, D. Frausto-Silva, J. L. Gutiérrez-Díaz, D. Domínguez, H. Tiznado and A. K. Cuentas-Gallegos, Effect of oxygen based functional groups on the nucleation of TiO2 by atomic layer deposition: A theoretical and experimental study, *Mater. Chem. Phys.*, 2021, 267.
33 K. Bernal Ramos, G. Clavel, C. Marichy, W. Cabrera, N. Pinna and Y. J. Chabal, In situ infrared spectroscopic study of atomic layer-deposited TiO2 thin films by nonaqueous routes, *Chem. Mater.*, 2013, **25**(9), 1706–1712.
34 H. H. Sønsteby, A. Yanguas-Gil and J. W. Elam, Consistency and reproducibility in atomic layer deposition, *J. Vac. Sci. Technol., A*, 2020, **38**(2), 020804.
35 R. H. J. Vervuurt, W. M. M. Kessels and A. A. Bol, Atomic Layer Deposition for Graphene Device Integration, *Adv. Mater. Interfaces*, 2017, **4**, 1700232.
36 A. González Vázquez, *Modelación a partir de principios fundamentales de las perovskitas Na0.5Bi0.5TiO3 y BiFeO3*, Master's thesis, Centro de investigación en materiales avanzados de Chihuahua, 2016, **http://cimav.repositorioinstitucional.mx/jspui/handle/1004/849**.
37 M. E. V. Macías, *Estudio por primeros-principios de la superficie de cromo (001) inducida con nitrógeno*, Master's thesis, Centro de Investigación Científica y de Educación Superior de Ensenada, Baja California, 2020, **https://cicese.repositorioinstitucional.mx/jspui/handle/1007/2804**.
38 A. A. Ali and A. M. Hashim, Density Functional Theory Study of Atomic Layer Deposition of Zinc Oxide on Graphene, *Nanoscale Res. Lett.*, 2015, **10**(1), 1008.
39 W. Koch and M. Holthausen, *A Chemist´s Guide to Density Functional Theory*, Wiley-VCH, 2nd edn, 2001, pp. 3–27.
40 A. González Vázquez, *Modelación a partir de principios fundamentales de las perovskitas Na0.5Bi0.5TiO3 y BiFeO3*, Master's thesis, Centro de investigación en materiales avanzados de Chihuahua, 2016, **http://cimav.repositorioinstitucional.mx/jspui/handle/1004/849**.
41 A. Echeverri, C. Cárdenas, M. Calatayud, C. Z. Hadad and T. Gomez, Theoretical analysis of the adsorption of ammonia–borane and their dehydrogenation products on the (001) surface of TiC and ZrC, *Surf. Sci.*, 2019, **680**, 95–106.
42 P. Giannozzi, S. Baroni, N. Bonini, M. Calandra, R. Car, C. Cavazzoni, D. Ceresoli, G. L. Chiarotti, M. Cococcioni,

I. Dabo, A. D. Corso, S. de Gironcoli, S. Fabris, G. Fratesi, R. Gebauer, U. Gerstmann, C. Gougoussis, A. Kokalj, M. Lazzeri, L. Martin-Samos, N. Marzari, F. Mauri, R. Mazzarello, S. Paolini, A. Pasquarello, L. Paulatto, C. Sbraccia, S. Scandolo, G. Sclauzero, A. P. Seitsonen, A. Smogunov, P. Umari and R. M. Wentzcovitch, *J. Phys.: Condens. Matter*, 2009, **21**, 395502.

43 P. Giannozzi, O. Andreussi, T. Brumme, O. Bunau, M. B. Nardelli, M. Calandra, R. Car, C. Cavazzoni, D. Ceresoli, M. Cococcioni, N. Colonna, I. Carnimeo, A. D. Corso, S. de Gironcoli, P. Delugas, R. A. DiStasio, A. Ferretti, A. Floris, G. Fratesi, G. Fugallo, R. Gebauer, U. Gerstmann, F. Giustino, T. Gorni, J. Jia, M. Kawamura, H.-Y. Ko, A. Kokalj, E. Küçükbenli, M. Lazzeri, M. Marsili, N. Marzari, F. Mauri, N. L. Nguyen, H.-V. Nguyen, A. O. de-la Roza, L. Paulatto, S. Poncé, D. Rocca, R. Sabatini, B. Santra, M. Schlipf, A. P. Seitsonen, A. Smogunov, I. Timrov, T. Thonhauser, P. Umari, N. Vast, X. Wu and S. Baroni, *J. Phys.: Condens. Matter*, 2017, **29**, 465901.

44 J. P. Perdew and Y. Wang, *Phys. Rev. B*, 1992, **45**, 13244–13249.

45 D. Vanderbilt, *Phys. Rev. B*, 1990, **41**, 7892–7895.

46 S. Grimme, Semiempirical GGA-Type Density Functional Constructed with a Long-Range Dispersion Correction, *J. Comput. Chem.*, 2006, **27**, 1787–1799.

47 G. Yang, L. Li, W. B. Lee and M. C. F. Ng, Structure of graphene and its disorders: a review, *Sci. Technol. Adv. Mater.*, 2018, **19**(1), 613–648.

48 Q. Xu, D. Prendergast and J. Qian, Real-Space Pseudopotential Method for the Calculation of 1*s* Core-Level Binding Energies, *J. Chem. Theory Comput.*, 2022, **18**(9), 5471–5478.

49 A. Aliano and G. Cicero, Ab Initio DFT Simulations of Nanostructures, in *Encyclopedia of Nanotechnology*, ed. Bhushan B., Springer, Dordrecht. 2012, pp. 11–17.

50 Di Wu, M. Tai, J. Zhou, Li. Chen, Ma. Guobin, G. Lu, M. Xia and Z. Gu, Effect of Substrate symmetry on the dendrite morphology of MoS2 Film synthesized by CVD, *Sci. Rep.*, 2017, **1**(7), 15166.

51 A. Loaiza, E. Araujo-López, J. Urresta and L.-R. Mario, Estudio computacional por DFT de la superficie (001) de WO3 tetragonal (P4/nmm), *Ing. Compet.*, 2018, **83**(20), 83–94.

52 G. Henkelman, B. P. Uberuaga and H. Jónsson, A Climbing Image Nudged Elastic Band Method for Finding Saddle Points and Minimum Energy Paths, *J. Chem. Phys.*, 2000, **113**, 9901–9904.

53 N. Ghaderi and M. Peressi, First-Principle Study of Hydroxyl Functional Groups on Pristine, Defected Graphene, and Graphene Epoxide, *Phys. Chem. C*, 2010, **114**, 21625–21630.

54 L. M. Mohlala, T.-C. Jen and P. A. Olubambi, Thermal stability and reactivity of titanium halide precursors for the atomic layer deposition of TiO 2 on a Pt (111) surface, *Procedia CIRP*, 2020, **93**, 9–13.

55 M. E. Dufond, M. W. Diouf, C. Badie, C. Laffon, P. Parent, D. Ferry, D. Grosso, J. C. S. Kools, S. D. Elliott and L. Santinacci, Quantifying the Extent of Ligand Incorporation and the Effect on Properties of TiO2 Thin Films Grown by Atomic Layer Deposition Using an Alkoxide or an Alkylamide, *Chem. Mater.*, 2020, **32**(4), 1393–1407.

56 X. Qi, Y. Jiang, D. Christophe, D. Davy, R. Van Meirhaeghe, G. Ru, Li Bing-Zong and X. Qu, Atomic layer deposition of TiO2 from tetrakis-dimethyl-amido titanium or Ti isopropoxide precursors and H_2O, *J. Appl. Phys.*, 2007, **102**, 083521.

57 R. A. Hackler, G. Kang, G. C. Schatz, P. C. Stair and R. P. Van Duyne, Analysis of TiO_2 Atomic Layer Deposition Surface Chemistry and Evidence of Propene Oligomerization Using Surface-Enhanced Raman Spectroscopy, *J. Am. Chem. Soc.*, 2019, **141**(1), 414–422.

58 Z. Hu and C. Heath Turner, Initial Surface Reactions of TiO_2 Atomic Layer Deposition onto SiO_2 Surfaces: Density Functional Theory Calculations, *J. Phys. Chem. B*, 2006, **110**, 8337–8347.

59 T. Promjun, T. Rattana and P. Pungboon Pansila, Kinetic study on initial surface reaction of titanium dioxide growth using tetrakis(dimethylamino)titanium and water in atomic layer deposition process: Density functional theory calculation, *Chem. Phys.*, 2022, **562**(2022), 111653.

60 Z. Hu and C. Heath Turner, Atomic Layer Deposition of TiO2 from TiI4 and H2 O onto SiO2 Surfaces: *Ab Initio* Calculations of the Initial Reaction Mechanisms, *J. Am. Chem. Soc.*, 2007, **129**, 3863–3878.

61 J. Guerrero-Sánchez, H. A. Borbon-Nunez, H. Tiznado and N. Takeuchi, Understanding the first half-ALD cycle of the ZnO growth on hydroxyl functionalized carbon nanotubes, *Phys. Chem. Chem. Phys.*, 2020, **22**, 15333–15339.

62 E. R. Johnson, S. Keinan, P. Mori-Sanchez, J. Contreras, A. J. Cohen and W. Yang, Revealing Noncovalent Interactions, *J. Am. Chem. Soc.*, 2010, **132**(18), 6498–6506.